GEOCHEMISTRY AND TECTONIC SIGNIFICANCE OF BASALTS IN THE DARE-ANAR COMPLEX: EVIDENCE FROM THE KAHNUJ OPHIOLITIC COMPLEX, SOUTHEASTERN, IRAN

M. Arvin[1][*], A. Houseinipour[1], A. A. Babaei[2] and H. A. Babaie[3]

[1] *Department of Geology, College of Sciences, Shahid Bahonar University, P. O. Box 133-76135, Kerman, Islamic Republic of Iran*
[2] *Department of Biological, Geological and Environmental Sciences, Cleveland State University, Cleveland, OH 44115, USA*
[3] *Department of Geology, Georgia State University, Atlanta, GA 30303, USA*

Abstract

The Kahnuj ophiolitic complex, a part of the Jazmurian ophiolitic belt, is located on the western boundary of the Jazmurian depression and is bounded by two major fault systems. There is a well-preserved, ophiolite pseudostratigraphy of early Cretaceous to early Palaeocene age and has a bearing on the Mesozoic development of southeastern part of Iran and adjacent region. The Kahnuj ophiolitic complex consists mainly of lava flows and pillow lavas with intermittent pelagic limestones, sheeted dykes, gabbros, and plagiogranites, with subordinate ultramafic rocks. Structurally, the complex is extensively faulted and fractured. The volcanic rocks have undergone low grade alteration and metamorphism, exhibiting greenschist facies assemblages. The basalts exhibit variable enrichment in LFS elements (Sr, K, Ba) relative to HFS elements (Ti, Zr, Y, Nb, P). The basalts are characterized by low Zr/Y (3.24-5.03), Th/Ta (1.29-2.55), La/Nb (1.43-2.15) and Nb/Y (0.12-0.2) ratios, relatively low TiO_2 and P_2O_5, and progressively enriched normalized patterns and increased Ce and Th values. Based on chemical discrimination parameters, the Dare-Anar basalts were originally developed in a back-arc basin and are representative of supra-subduction zone Tethyan ophiolites.

Introduction

Ophiolites, as remnants of obducted oceanic crust, mark, the presence of former suture zones and play an important role in plate tectonic reconstructions [9,33] Mesozoic ophiolites are widespread in Iran and Middle-East region (e,g, Vourinos, Troodos, Baer-Bassit, Neyriz, Semail). They represent the variably disrupted fragments of the Neotethyan ocean that developed during the Triassic between Eurasia and Gondwanaland [6,54,55]. The Mesozoic suture zones in Iran are marked by significant areal disruption of ophiolite-related bodies. These suture zones are interpreted by

[*] *E-mail: arvin@arg3.uk.ac.ir*

numerous models. Ricou [46] considered them as originating from a single ocean while others believe that separate ophiolites alignments represent different ocean basins [6,25]. This latter view is more consistent with different magmatic affinity of the various Iranian Mesozoic ophiolitic complexes.

A tentative tectonic reconstruction (Fig. 1) suggests that the Iranian Neotethyan ophiolites formed in three different structural zones: two allochthonous (1 and 2), and one authochthonous to parauthochthonous (3) which were derived from separate ocean basins. Those structural zones are: (1) a southern northwest-southeast trending belt which is called the Peri-Arabic belt [46] or southern Neotethyan ocean [53,55], (2) the Central Iranian belt (trending N-S and E-W) which represents remnants of the Nain-Baft, Sabzevar and Sistan oceans [32,63], and (3) the Jazmurian belt which trends northwest and east-west marking the remnants of Makran ocean (Inner Makran suture of McCall and Kidd, [32]). The well preserved Kahnuj ophiolite belongs to this belt.

Most of the information available up to now on the large ophiolitic belt south of the Jazmurian depression has come from the large scale geological mapping of southeastern Iran by Paragon Contech Consulting geologists on contract for the Geological and Mineralogical Survey of Iran [31] and also as part of a regional geological interpretation [11,13,32]. This paper considers the petrochemistry of the basaltic rocks from Dare-Anar complex, and in particular determines their petrogenesis and initial eruptive environment within the Kahnuj ophiolitic complex. Also, in the broader context of the origin of ophiolites to determine if the Dare-Anar basalts are remnants of ancient ocean floor, or in the light of the duality of Tethyan ophiolites in particular [38,48], formed above a subduction zone. The data represented here were obtained through a detailed study of the ophiolitic mélange belt in the Kerman province [3,4] and southern Jazmurian depression.
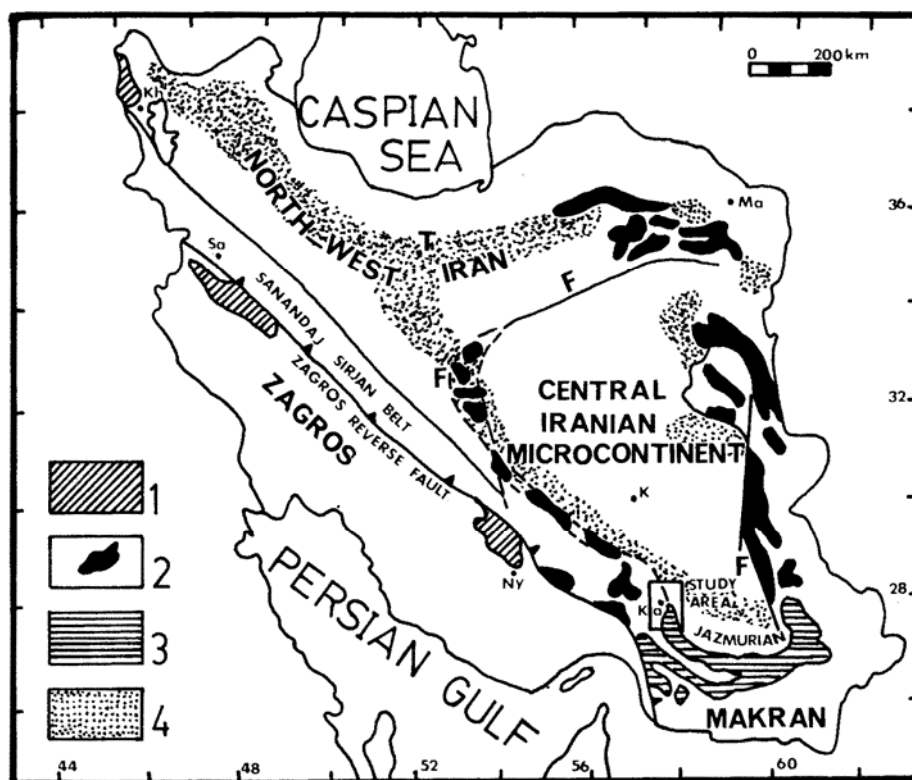
Figure 1. Map showing the distribution of the Iranian Mesozoic ophiolites: 1- Peri-Arabic belt, 2- Central Iranian belt, 3- Jazmurian belt, 4- Maastrichtian-Paleogene volcanic rocks. Ka=Kahnuj; Kh=Khoy; Ma=Mashhad; Ny=Neyriz; Sa=Sanandaj; T=Tehran.
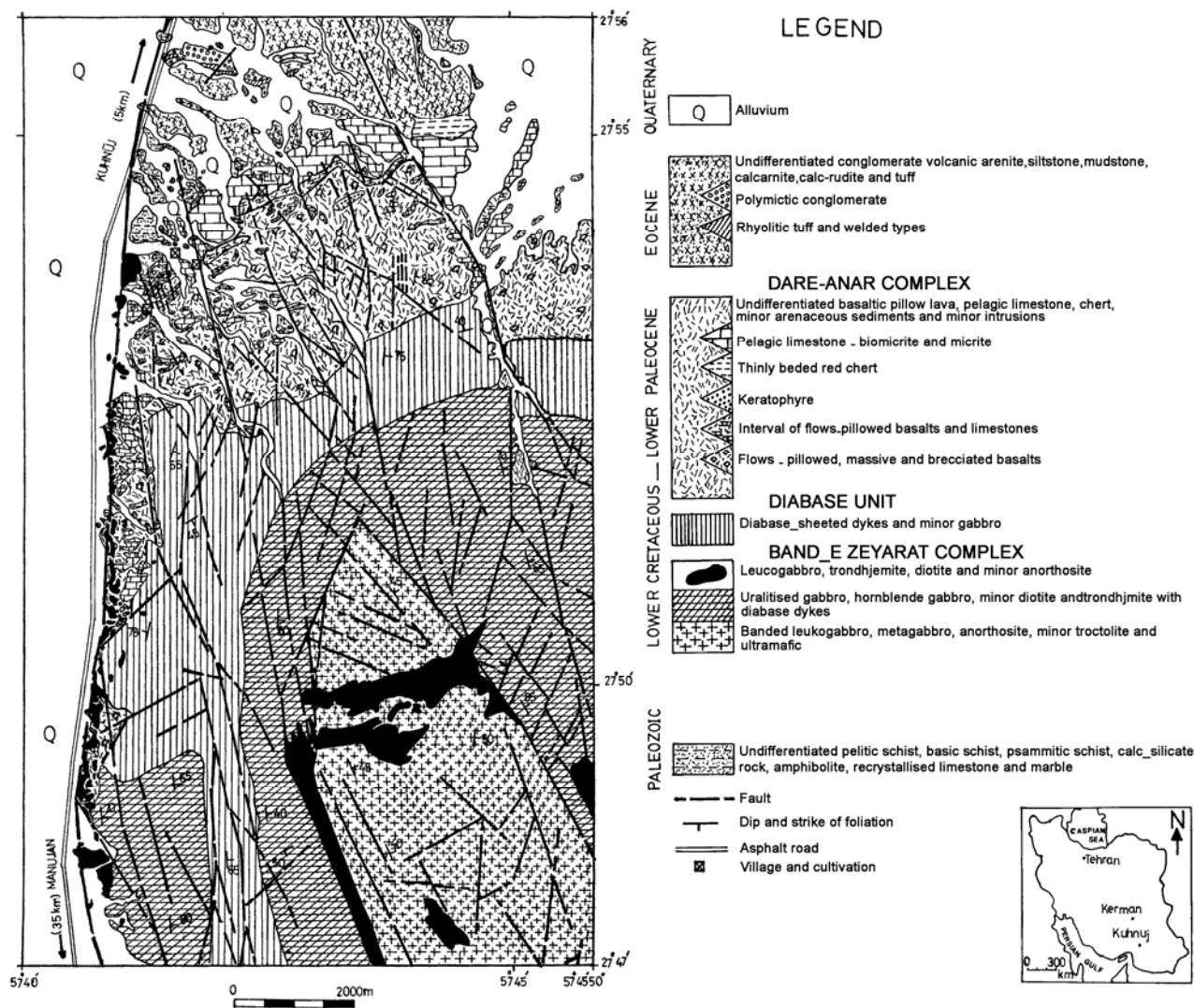
Figure 2. Geological map of the Kahnuj ophiolitic complex, southeast of Kahnuj, Kerman (modified from the Geological Map of Iran, 100,000 Series, sheet 7545).

Field Relationships and Features

The Kahnuj ophiolitic complex lies in the Inner Makran marginal basin [32] in southern Iran (Fig. 1). An area of about 160 km^2 has been mapped on a scale of 1:20,000, with a main providing detailed information on structural and stratigraphic relationships within the complex (Fig. 2). Although the normal, well-preserved ophiolite pseudostratigraphy of lava flows, pillow lavas, sheeted dykes, plagiogranites and gabbros is present, voluminous ultramafics are not exposed in this section of the Jazmurian ophiolitic belt. The Kahnuj ophiolite is bounded to the east and west by two major north-south trending fault zones (Fig. 2). Structurally the complex is extensively faulted and fractured. The field relationships and fauna of ophiolite-related sediments indicate that the Kahnuj ophiolite is early Cretaceous to early Palaeocene in age.

The ophiolite sequence is divided into three distinct units: (a) a plutonic (Bande-Zeyarat) complex, (b) diabase sheeted dykes, and (c) a volcanic (Dare-Anar) complex (Fig. 2). The severe faulting and hydrothermal alteration near the contact between high- and low-level gabbros obscures their original relationships, although it is thought to have been transitional [31]. The plutonic complex for the most part is divided into the banded low level gabbro and the high level gabbros based on their field appearance and petrography. The low-level gabbro consists of cumulate banded gabbro, olivine gabbro and leuco-gabbro, anorthosite, minor troctolite and pegmatoid and tectonic rafts of dunite, A steep, east-dipping banding and rhythmic layering is developed in the low-level gabbros.

The high-level gabbro has a low weathering profile and is composed of non-cumulate gabbro with xenomorphic textures. Uralitised gabbro, hornblende gabbro, hornblende pegmatoid and minor dunite in it are altered and decomposed. The Bande-Zeyarat complex is a part of a classic ophiolite sequence of plutonic rocks, cumulate layered in the lower part and non-cumulate above. The gabbro is cut by a set of north-south trending dykes. These bodies comprise a set of sub-vertical doleritic sheeted dykes (98% of the rock mass) and occupy a total area of about 2-2.5 km^2. The isolated dykes show symmetrical chilled margins, but sheeted dyke complex show typical asymmetrical chilled margins and their width varies from 0.5 to 5 m.

There are leucocratic bodies of trondhjemitic plagiogranites within the ophiolitic complex forming irregular or sheet-like bodies, tens or hundreds of meters across which cut through the whole complex. Silicic dykes which occur locally within the high-level gabbro and above the sheeted dyke complex, appear to be genetically part of the ophiolite complex.

The eruptive rocks of the Dare-Anar complex, outcrop in a discontinuous zone up to 3-4 km wide. The extensively faulted, fractured and deformed nature of Dare-Anar complex, makes any section measuring meaningless. The volcanic rocks (approximately 10×4 km^2) are mainly composed of basaltic and basaltic-andestic pillow lavas with subordinate interbedded massive lava flows, and associated pillow breccias. The massive flows show gentle flexuring. Vesicular, amygdaloidal and variolitic textures are common in these rocks. Vesicles (up to 3 cm in diameter) are filled mainly by calcite, quartz, chlorite and epidote. The massive and pillowed flows are predominantly greyish-green to light green in colour, reflecting the proportion of secondary minerals, whereas reddish-brown flows are the result of subsequent oxidation. The pillow lavas form a pile of draped ellipsoidal to elongate tubes and vary in diameter from 0.15 to 3 m. Keeping their geopetal structure, the pillow lavas are highly vesicular at the top part of each pillow lava tube. Their original glassy margins are now mostly palagonitized whereas the interiors are holocrystalline and often less vesicular. Individual flows can be distinguished by their brecciated margins and the presence of interlayered thinly bedded pelagic limestone. The limestone, consisting of pelagic micrite and biomicrite, is often associated with red chert and sandstone which are sometimes interbedded with pillow lava. The limestone is in depositional contact with basaltic rocks and becomes more abundant towards the top of the Dare-Anar complex. It contains pelagic microfaunas (*Globigerinelloides* sp. and *Hedbergella* sp.) of Aptian-Cenomanian age. A few outcrops of keratophyres, up to 10 m wide, also occur between the basaltic flows. Their pronounced fluidal (trachytic) textures are defined by 1-2 mm long plagioclase crystals.

Petrography

The gabbro in the Kahnuj ophiolite generally preserves igneous textures and original mineral phases. In contrast to the low-level gabbro, most of the high-level gabbro is altered to greenschist facies assemblages of uralite, saussuritised plagioclase, epidote, chlorite and quartz. The doleritic dykes are porphyritic to non-porphyritic with glomeroporphyritic, intergranular to subophitic textures. They consist mainly of plagioclase (oligoclase to labradorite, often saussuritized), pyroxene (typically uralitized), ilmenite and titanomagnetic minerals. Chlorite, prehnite, epidote, sphene, calcite and quartz occur as secondary minerals.

The basalts are aphyric to weakly porphyritic rocks with plagioclase and subordinate clinopyroxene as phenocryst phases. In many of the basalts the primary minerals and textures are strongly overprinted by secondary assemblages produced during initial ocean-floor hydrothermal alteration. However, most of the primary textures related to cooling history (e.g. variolitic, intersertal, pilotaxitic and intergranular) have been preserved. The affects of alteration are secondary assemblages of albite, chlorite, calcite, epidote, zeolite, quartz, prehnite, sphene, iron oxide and actinolite (metabasalts). Albite replaces both phenocrysts and matrix laths, whereas chlorite commonly occurs in the matrix, apparently replacing original glass. The volcanic rocks have highly variable vesicularities, 0-70% by volume, which suggests variable but generally shallow eruption depth probably less than 500 m below sea level [34,35]. Vesicles were originally infilled with calcite, chlorite and quartz along with epidote and zeolites as separate fan-shaped aggregates (up to 4-5 cm in diameter). Prehnite occurs chiefly in veins. Uralite is also an abundant alteration phase and occurs as scattered fibers throughout the matrix or replacing pyroxenes. The dominant secondary assemblages (both in basalt and dolerite dykes) indicate that the rocks gone through zeolite to greenschist facies metamorphism. However, late circulation of low temperature fluids is reflected by the development of veinlets and vesicle-filling quartz and carbonates replacing earlier alteration phases. Petrographically and chemically (see below), the basalts of the Kahnuj ophiolite are very similar to basaltic rocks formed along mid-oceanic ridges (MORB) and marginal basins, which are characterized by the crystallization order of olivine, plagioclase and clinopyroxene [8,43,71]. The keratophyre have well-developed trachytic textures and are composed of plagioclase, quartz, chlorite, epidote, calcite, sphene and opaque minerals. Trondhjemite occur as fine to

intermediate hypidiomorphic granular to subophitic rocks composed of turbid plagioclase (albite to andesine), quartz, hornblende, with accessory sphene and zircon. The trondhjemite is overprinted by greenschist facies assemblages. The zone of intrusion by trondhjemite is marked by pronounced hydrothermal alteration.

Analytical Methods

The samples analysed were finely powdered in an agate mill. Major element analyses were performed in the Department of Geology at Georgia State University. They were measured by a wavelength dispersive, Rigaku 3070 XRF spectrometer utilizing a side-window Rhodium, target X-ray tube. Analyses were performed on fused glass disks using nine parts lithium borate flux and one part rock powder, and heating in a furnace at 1000°C. The REE and trace element analyses were performed in the College of Oceanic and Atmospheric Sciences at Oregon State University, Analyses of trace elements were performed by the Varian ICP-AES. About 0.1 g of the sample powder was mixed with 0.9 g lithium borate flux in a carbon crucible and heated in a furnace at 1100°C for 30 min. The fused glass samples were dissolved (using a magnetic stirring device) in 100 ml of 1% HNO_3 solution with Germanium as internal standard. International basalt standards such as BCR-1 were chosen for calibration.

The rare earth elements (REE), Hf, Ta, Th and Nb were determined by inductively coupled plasma mass spectrometry (ICP-MS) techniques. The sample powder (0.08 g) were dissolved, using a mixture of HF, HCl and HNO_3 in special screw-top plastic vials. An internal standard solution containing Indium element was then added and the spiked sample dissolutions were diluted with 1% HNO_3. The internal standard was used for monitoring drift in mass response during mass spectrometric measurements. Dissolution of BCR-1, W2, IB-1a and BIR-1 were chosen as calibration standards for element concentrations of the measured samples [18].

Representative basaltic rocks (50 samples) were collected from lava flows and pillow lavas and eventually 27 samples, were analyzed for major selected trace elements, with a subset of 11 samples being determined for rare earth elements (REE), Hf, Ta, Th and Nb. The representative analyses are shown in Table 1.

Geochemistry of the Ophiolites
Major and Trace Elements

All samples used in this study have undergone, some degree of low-grade alteration and metamorphism (zeolite-greenschist), a feature typical of other ophiolite basalts [42,44,57,64]. The wide variation in loss-on-ignition (LOI) values (Table 1) is a crude measure of the

degree of alteration and reflects the contribution by secondary hydrated and carbonate phases. Samples with chlorite and oxidation products as the main secondary phase can have LOI-values up to ~5 wt% whereas in further degradation, which generally involves late carbonation and zeolitization increases LOI to 10 wt% in extreme cases. Because of documented mobility of many elements during low grade submarine alteration [19,22,28,30,62,68] the variation exhibited by most major oxides and low field strength (LFS) trace elements, such as Ba, Sr are unlikely to reflect primary composition in the Dare-Anar basalts. For altered volcanics, recourse is generally made to relatively "immobile" elements such as Ti, P, Zr, Y, Nb and REE and to lesser extent Cr, Ni, Sc and V, to designate petrogenetic trends and tectonic environments [16,42, 52,58]. In a similar manner, the normalized REE data develop smooth patterns of variation (see later) that are considered typical of their original composition. However, under some conditions, such as extensive carbonation of the lavas or severe sea floor-hydrothermal alteration, the REE and HFSE can be mobilized and/or abundances diluted [20,21,23,26, 37,45,61,71]. As the Dare-Anar basalts exhibit a range of mineralogical reconstruction from mild to extreme, three general chemical alteration classes are defined on the basis of LOI-values at <5 wt% (mild alteration, coded 1), 5-8 wt% (strong alteration, coded 2) and >8 wt% (severe alteration, coded 3). In this study samples with >8 wt% LOI (alteration coded 3) were avoided.

The components that are mobile during alteration (e.g. Ba) exhibit scattered non-magmatic distributions, whereas generally immobile element (e.g. Ti, Y) have characteristic linear relationships, relative to Zr (Fig. 3). On the basis of relatively immobile trace elements, the Dare-Anar basalts show the following characteristics: low Zr/Y (3.24-5.03) Th/Ta (1.29-2.55), La/Nb (1.43-2.15) and Zr/Nb (18-29) ratios, low Nb/Y ratios (0.12-0.2) characteristics of sub-alkaline (tholeiitic) basalts [69], a wide range of Cr and Ni contents (together with variable FeO*/MgO ratios), relatively low TiO_2, P_2O_5 contents and low TiO_2/P_2O_5 ratios (4.70-8.82) characteristics of transitional tholeiites [59], features that are also shown by basalts from Shikoku basin [27]. Overall the preliminary data indicate that the volcanic rocks represent a moderately differentiated magma, involving mafic and oxide phases. Chemical discrimination of the eruptive environment for basic rocks, using such diagrams as displayed in Figure 4, suggests that the Dare-Anar basalt lavas have affinities with typical mid-ocean ridge basalts (MORB) and back-arc basin basalts (BABB), rather than island-arc tholeiite (IAT) [39,50]. On the Cr-Y covariation of Pearce [39] (Fig. 4c), 15-30% partial melting of plagioclase lherzolite is needed

to produce the Dare-Anar basalt composition. Relatively low contents of Cr in some of the Dare-Anar basalts may suggest that the magma source underwent an earlier phase of fractionation.

The Ce/Nb versus Th/Nb diagram (Fig. 5) is considered to the best discriminant of tectonic environment and these ratios are interpreted to reflect source values [52]. In Figure 5, the Dare-Anar basalts plot in the field of back-arc basalts, with a trend towards the average of continental crust. The La/Nb ratio provides an indicator of LILE-enrichment in a subduction-elated environment relative to HFSE [15]. As seen in Figure 6, the La/Nb ratio, together with Y, provides a useful discriminant between ocean ridge (with low, restricted La/Nb) and subduction-related eruptive settings [7,15]. The moderate La/Nb ratios of the Dare-Anar basalts indicate that they are probably representative of a back-arc basin environment (rather than an arc) and are clearly distinguished from enriched MORB or intraplate oceanic sheet-flows with similar low Y contents [14].
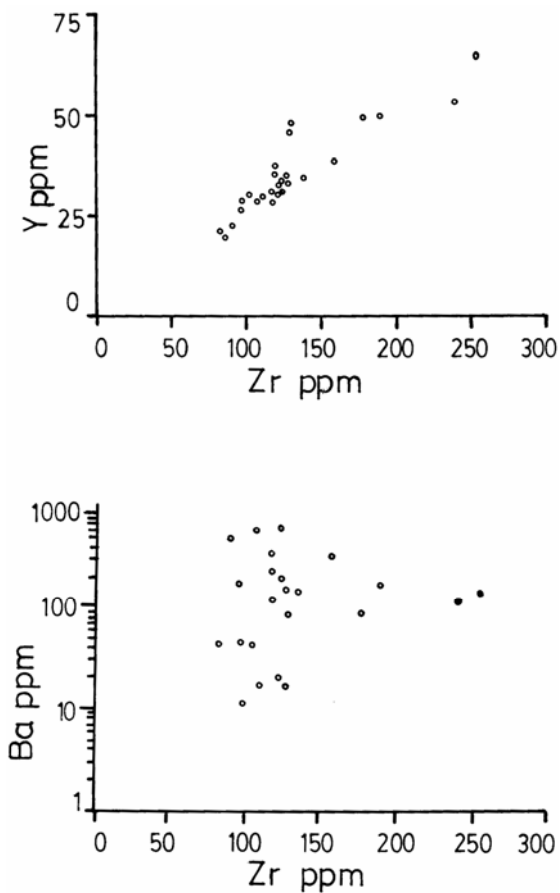
Figure 3. Variations of mobile (Ba) and immobile (Y) elements relative to Zr for the Dare-Anar basaltic from the Kahnuj ophiolitic complex.
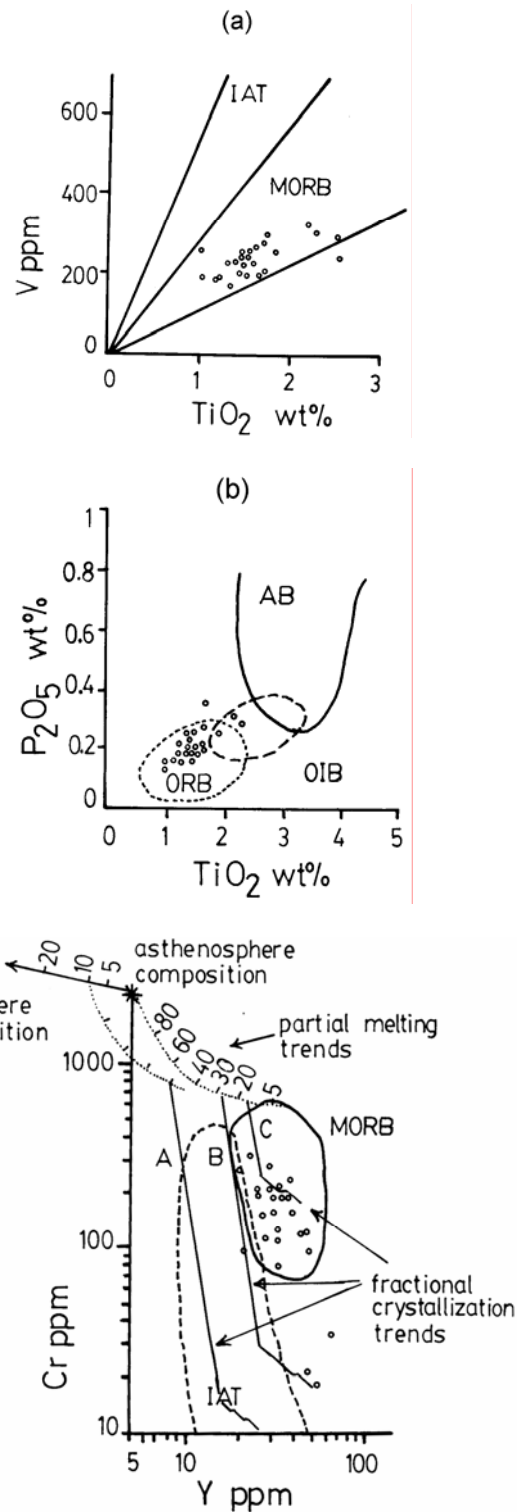
Figure 4. Chemical discrimination of Dare-Anar basalts from the Kahnuj ophiolitic complex. IAT=Island arc tholeiite field; MORB=Mid-ocean ridge basalt field; AB=alkali basalts field; OIB=Ocean-island tholeiites field. V-TiO_2 diagram from Shervias [56], Cr-Y diagram from Pearce *et al.* [43], P_2O_5-TiO_2 from Bass *et al.* [5].
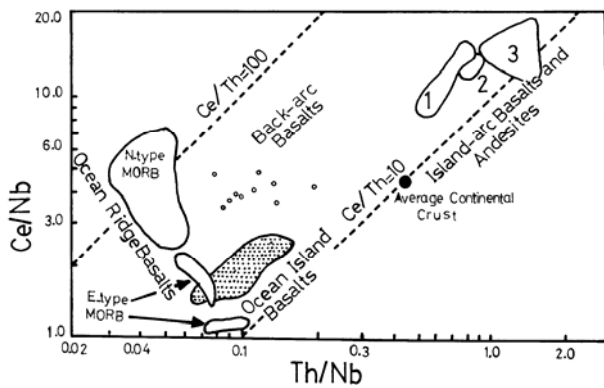
Figure 5. Ce/Nb versus Th/Nb diagram for the Dare-Anar basalts from the Kahnuj ophiolitic complex, fields are from Saunders and Tarney [52]. 1-Ascension, 2-Agrigan, 3-Seamount, N. Mariana arc.
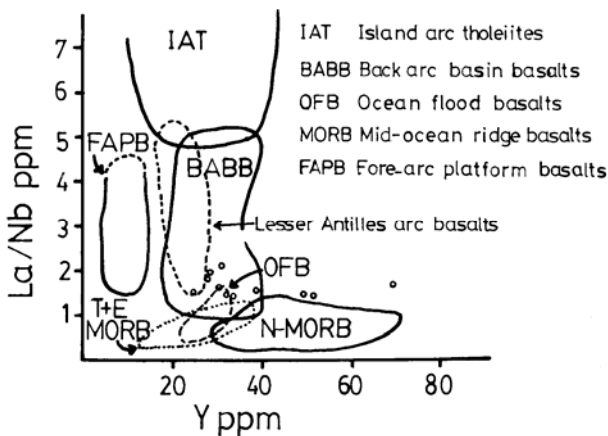
Figure 6. La/Nb-Y plot [15] for the Dare-Anar basalts from the Kahnuj ophiolitic complex.

The trace element pattern for basalts normalized to N-type MORB composition is also a useful guide to magma type tectonic environment [38,39,41,43]. A N-type MORB normalized, multi-element diagrams (Fig. 7) for the Dare-Anar basaltic rocks show similar enrichment patterns to selected back-arc basin basalts from both ensialic and ensimatic settings, with little Th enrichment [43,52]. Within the LIL element group, Th is a relatively stable and reliable indicator, whose enrichment relative to other incompatible elements is taken to represent the subduction zone component [40,70].

The chondrite-normalized rare earth element (REE) patterns for Dare-Anar basalts (Fig. 8) show a mild enrichment in the LREEs relative to HREEs. The generally smooth normalized pattern with light REE (LREE) enrichment shown by the Dare-Anar basalts is characteristics of magmatic suits unaffected by alteration. As seen in Figure 8, the normalized REE
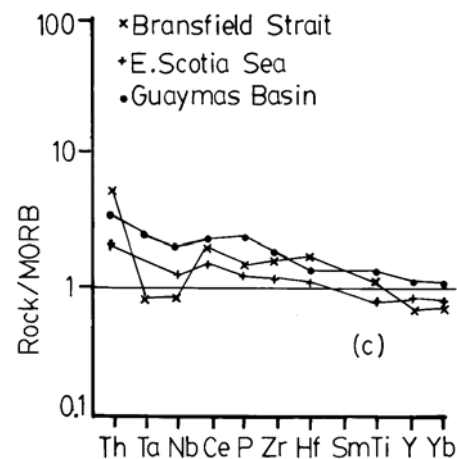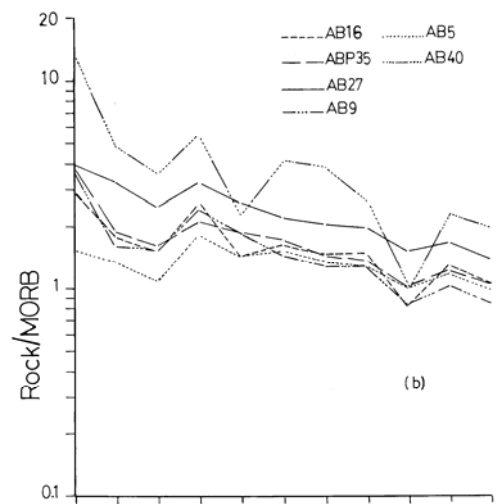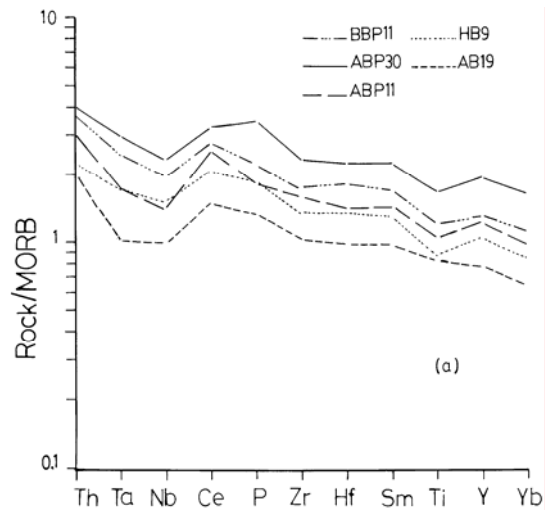
Figure 7. MORB-normalized (values from Saunders and Tarney, [52]) multi-element plots for the Dare-Anar basalts [diagrams (a) and (b)], compared with selected back-arc basin basalts [diagram (c)] from Bransfield strait (Weaver *et al.* [65]), E. Scotia Sea (Saunders and Tarney, [51]) and Guaymass basin, Gulf California (Saunders *et al.* [50]).
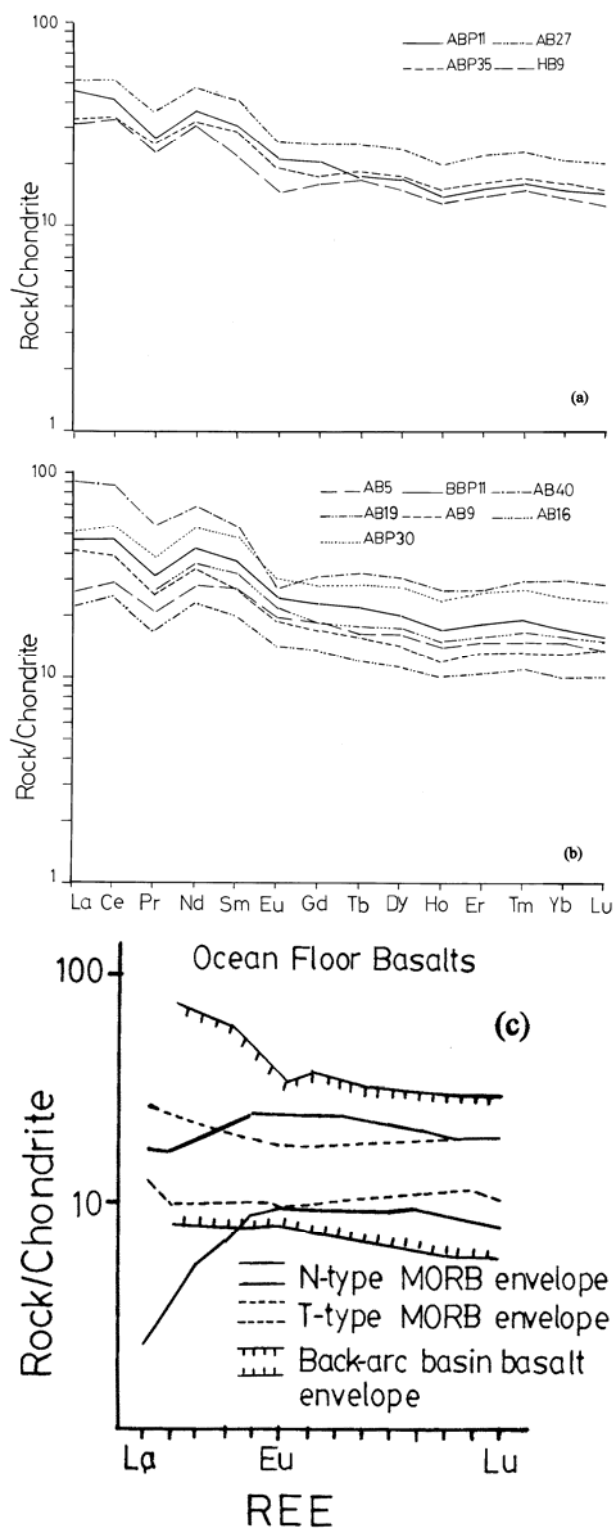
Figure 8. Chondrite-normalized REE patterns for the Dare-Anar basalts from the Kahnuj ophiolitic complex [diagrams (a) and (b)] (normalization factors from Newpet 2), and comparison with N-MORB envelope [17,49]), T-MORB envelope (FAMOUS data [66,67]) and back-arc basin basalt envelope, BABB (Saunders and Tarney [51,60]) [diagram (c)].

patterns lack the LREE depletion typical of N-type MORB (and many arc tholeiitic, IAT) although they have similarities to T-type MORB and some back-arc basin basalts (BABB) [24,59]. The absence of a distinct Eu anomaly in the Kahnuj basalts also suggests that plagioclase fractionation was not particularly significant, or may indicate that the magma was relatively oxidized.

Discussion and Conclusion

The Kahnuj ophiolite is one of the best preserved and intact ophiolite pseudostratigraphic complexes in the Neotethys ophiolitic belt. Geochemical data indicate that the Dare-Anar basalts are tholeiitic in composition and have similarities to transitional MORB tholeiites and some marginal basin basalts. The basaltic lavas were probably formed by approximately 15-30% partial melting of mantel material.

The Neotethys was developed during the Late Paleozoic to Middle Triassic between Gondwana and the continental blocks of Iran and Afghanistan which became separated from Gondwana and collided with Europe [10]. This was followed by multibranch rifting and development of narrow ocean basins (as branches of Neotethys) throughout the Late Jurassic-Early Cretaceous interval. Late Cretaceous compression resulting from convergence between Africa and Europe led to the narrowing of the Neotethys and eventually closure of its different branches (e.g. Inner Makran) throughout Late Paleocene-Eocene interval, leading to emplacement/ or juxtaposition of central Iranian and Jazmurian ophiolitic belts.

The Tethyan ophiolites (extend from the western Mediterranean to the Persian Gulf and beyond) has been divided into two groups: (a) fragmented Jurassic ophiolites in the western and central area (e.g. Alps, Dinarides) and (b) mid to the Late Cretaceous ophiolites displaying a pseudostratigraphy at eastern end (e.g. Troodos, Semail) [1,36,48]. The first group displaying MORB-like features, whereas the second group exhibits SSZ features often comparable with younger back-arc basins worldwide [38,43,47]. Also based on their mode of emplacement, the Neotethyan ophiolites have been divided into thee types: Peri-Arabic, Ligurian and Makran, which accreted to continents by pure obduction (i.e. without collision), collision-related obduction, and simple juxtaposition respectively [25].

The Iranian ophiolitic complexes have been postulated to have formed in a variety of tectonic settings: such as mid-oceanic ridges, incipient ocean ridges, small oceanic basins such as the Red Sea, marginal basins, leaky transform faults and island arcs [2,3,4,6,12,13,32,63]. Faunal data from the Inner Makran indicate a Jurassic age for the initiation and development of a rifting which eventually led to the

Table 1. Analyses of representative of Dare-Anar basaltic rocks from the Kahnuj ophiolitic complex
Note: Major oxides in wt%; minor and trace elements in ppm; LOI=loss on ignition, FeO*=total Fe as FeO

Sample No.	AB5	AB9	AB12	AB13	AB16	AB19	AB22	AB25	AB26
Alteration Code	**1**	**1**	**1**	**1**	**3**	**2**	**1**	**1**	**1**
SiO_2	48.54	52.87	53.58	52.07	42.16	50.59	53.05	48.76	46.25
TiO_2	1.50	1.25	1.47	1.74	1.21	1.28	1.53	1.51	2.19
Al_2O_3	15.43	14.24	14.84	13.85	12.81	15.30	15.05	15.04	14.13
FeO*	10.19	6.60	7.08	7.53	6.49	7.09	8.94	8.75	11.60
MnO	0.18	0.13	0.16	0.19	0.14	0.15	0.18	0.15	0.21
MgO	6.86	4.58	4.15	2.46	3.15	5.23	3.23	4.21	4.91
CaO	8.01	7.56	6.37	8.53	18.43	7.58	5.44	8.81	8.98
Na_2O	3.05	4.62	4.62	5.40	3.23	3.80	6.32	6.74	2.40
K_2O	1.31	2.54	3.94	1.95	0.95	4.08	1.71	1.09	3.75
P_2O_5	0.17	0.22	0.25	0.37	0.17	0.16	0.26	0.21	0.33
LOI	3.37	4.53	2.19	4.64	10.73	5.19	2.79	4.45	3.91
Sum	98.61	99.14	98.65	98.73	99.47	100.45	98.50	100.08	98.66
Mg/Fe*+Mg	0.54	0.55	0.51	0.37	0.46	0.57	0.39	0.46	0.43
TiO_2/P_2O_5	8.82	5.68	5.88	4.70	7.12	8	5.88	7.19	6.64
Sc	38	28	30	26	28	28	25	35	36
Sr	519	163	337	91	77	645	82	229	782
Cr	296	157	196	n.d.	234	337	18	248	129
Ni	108	47	62	n.d.	184	138	36	119	45
Ba	618	359	207	143	47	498	110	226	167
Zr	111	118	123	254	97	91	241	120	180
Y	31	27	31	66	26	24	54	37	47
V	257	204	238	182	190	194	219	242	322
Nb	3.80	5.30			5.30	3.50			
La	6.30	9.80			9.60	5.30			
Ce	18.00	24.00			25.00	15.00			
Pr	2.80	3.40			3.70	2.30			
Nd	13.20	15.30			16.90	10.70			
Sm	4.10	4.10			4.90	3.10			
Eu	1.51	1.37			1.68	1.13			
Gd	5.05	4.52			5.02	3.72			
Tb	0.86	0.81			0.93	0.63			
Dy	5.57	4.82			6.01	3.85			
Ho	1.20	1.04			1.28	0.85			
Er	3.38	2.93			3.62	2.35			
Yb	3.23	2.79			3.49	2.26			
Tm	0.51	0.44			0.57	0.37			
Lu	0.47	0.45			0.53	0.34			
Hf	3.16	3.07			3.44	2.27			
Ta	0.24	0.29			0.31	0.19			
Th	0.31	0.74			0.57	0.42			
U	0.15	0.30			0.75	0.24			
Zr/Y	3.58	4.37	3.96	3.85	3.73	3.79	4.46	3.24	3.83
Ti/Zr	80.00	63.00	71.00	41.00	74.00	85.00	38.00	75.00	73.00
Zr/Nb	29.20	22.30			18.30	26.00			
La/Nb	1.65	1.85			1.81	1.51			
Th/Ta	1.29	2.55			1.84	2.21			
Nb/Y	0.12	0.20			0.20	0.14			
Th/Nb	0.08	0.14			0.11	0.12			

Table 1. Continued

Sample No.	AB27	AB32	AB40	ABP10	ABP11	ABP24	ABP30	ABP33	ABP35
Alteration Code	1	2	1	2	1	1	1	2	1
SiO_2	51.55	48.47	57.13	46.93	52.68	50.28	50.09	49.71	50.34
TiO_2	2.27	1.18	1.48	1.73	1.54	1.43	2.54	1.73	1.57
Al_2O_3	13.63	14.14	14.32	12.72	15.15	14.18	13.82	13.85	13.70
FeO*	9.26	6.67	8.73	8.89	6.87	8.64	11.02	7.61	8.11
MnO	0.16	0.14	0.13	0.17	0.33	0.13	0.16	0.13	0.13
MgO	3.99	4.29	3.76	5.48	3.53	3.00	3.06	2.73	4.33
CaO	7.73	9.83	4.63	10.28	6.16	10.76	8.27	9.91	8.47
Na_2O	5.64	3.58	4.86	5.01	3.07	4.90	7.75	4.48	6.98
K_2O	1.41	3.75	0.82	0.19	7.27	0.49	0.11	3.30	0.94
P_2O_5	0.31	0.19	0.27	0.24	0.22	0.21	0.42	0.30	0.22
LOI	3.26	6.33	3.09	6.93	2.77	4.71	3.18	5.23	4.45
Sum	99.21	98.57	99.22	98.57	99.59	98.73	100.42	98.95	99.24
Mg/Fe*+Mg	0.42	0.53	0.43	0.52	0.50	0.38	0.33	0.39	0.49
TiO_2/P_2O_5	7.23	6.21	5.48	7.21	7.00	6.81	6.05	5.67	7.14
Sc	33	29	24	30	33	27	29	27	33
Sr	100	295	78	169	287	115	74	156	239
Cr	127	197	34	130	233	234	97	22	196
Ni	145	89	105	40	135	125	189	46	51
Ba	91	193	64	15	819	43	n.d.	161	91
Zr	179	97	347	127	125	108	179	190	128
Y	48	26	69	34	31	30	50	50	34
V	298	190	194	279	238	218	250	193	242
Nb	8.50		12.30		5.10		8.20		5.50
La	12.20		21.00		11.00		12.00		7.90
Ce	32.00		53.00		25.00		33.00		21.00
Pr	4.80		7.40		3.70		5.20		3.30
Nd	22.50		31.80		16.90		24.90		15.20
Sm	6.50		8.50		4.70		7.50		4.50
Eu	2.02		2.08		1.63		2.34		1.49
Gd	6.92		8.55		5.68		7.72		4.81
Tb	1.30		1.66		0.91		1.49		0.94
Dy	8.24		10.70		5.88		9.59		5.89
Ho	1.72		2.27		1.20		2.02		1.26
Er	5.00		6.69		3.44		5.87		3.63
Yb	4.62		6.66		3.26		5.57		3.49
Tm	0.75		1.08		0.54		0.91		0.57
Lu	0.70		1.00		0.49		0.83		0.52
Hf	4.83		9.11		3.37		5.42		3.45
Ta	0.59		0.85		0.32		0.55		0.33
Th	0.79		2.65		0.62		0.83		0.79
U	0.80		0.92		0.43		1.89		1.45
Zr/Y	3.73	3.73	5.03	3.73	4.03	3.60	3.58	3.80	3.76
Ti/Zr	76.00	73.00	26.00	82.00	74.00	80.00	85.00	54.00	73.00
Zr/Nb	21.00		28.20		24.50		21.80		23.30
La/Nb	1.43		1.70		2.15		1.46		1.43
Th/Ta	1.34		3.11		1.93		1.51		2.39
Nb/Y	0.18		0.18		0.16		0.16		0.16
Th/Nb	0.09		0.21		0.12		0.10		0.14

Table 1. Continued

Sample No.	BBP4	BBP11	BDB8	HB9	HP3-1	HP3-2	RBP2	RVB2	URBP2
Alteration Code	1	1	1	1	1	2	3	2	2
SiO_2	56.41	49.61	52.06	55.45	51.85	50.49	44.41	36.70	46.53
TiO_2	1.02	1.85	1.03	1.35	1.33	1.34	1.53	1.68	1.62
Al_2O_3	13.98	14.78	16.73	13.32	16.47	13.60	13.08	13.68	12.57
FeO*	7.13	9.43	7.23	6.62	7.54	8.01	6.89	10.83	6.98
MnO	0.18	0.16	0.15	0.13	0.13	0.13	0.14	0.12	0.14
MgO	8.03	6.61	4.50	4.56	4.65	3.82	4.70	4.92	3.96
CaO	7.27	8.51	9.14	8.23	6.53	11.82	14.26	22.45	12.85
Na_2O	5.29	3.42	5.34	5.41	5.66	3.99	4.51	0.86	4.43
K_2O	0.10	0.47	0.04	0.21	0.87	0.17	0.33	0.09	2.08
P_2O_5	0.17	0.27	0.14	0.23	0.23	0.21	0.21	0.22	0.23
LOI	1.28	4.46	2.14	4.76	4.31	5.63	9.05	7.90	7.79
Sum	100.86	99.57	98.50	100.27	99.57	99.21	99.11	99.45	99.18
Mg/Fe*+Mg	0.67	0.55	0.53	0.55	0.52	0.46	0.55	0.45	0.51
TiO_2/P_2O_5	6.00	6.85	7.35	5.87	5.78	6.38	7.28	7.64	7.04
Sc	28	31	28	28	35	28	33	34	34
Sr	234	346	358	126	298	153	158	37	122
Cr	256	161	95	79	183	158	113	105	190
Ni	116	60	35	37	55	101	41	38	72
Ba	49	345	n.d.	18	123	17	12	n.d.	156
Zr	84	160	79	126	120	102	98	118	136
Y	20	39	22	33	36	30	28	31	35
V	206	270	261	170	227	242	257	307	276
Nb		7.00		5.30					
La		11.00		7.60					
Ce		28.00		21.00					
Pr		4.20		3.10					
Nd		19.50		14.60					
Sm		5.70		4.40					
Eu		1.89		1.14					
Gd		6.26		4.46					
Tb		1.13		0.86					
Dy		6.87		5.26					
Ho		1.45		1.13					
Er		4.05		3.24					
Yb		3.78		2.97					
Tm		0.65		0.51					
Lu		0.53		0.44					
Hf		4.44		3.29					
Ta		0.45		0.32					
Th		0.76		0.46					
U		0.29		0.29					
Zr/Y	4.20	4.10	3.59	3.28	3.33	3.40	3.50	3.81	3.88
Ti/Zr	73.00	69.00	78	64.00	66.00	78.00	94.00	85.00	57.00
Zr/Nb		22.80		23.70					
La/Nb		1.57		1.43					
Th/Ta		1.69		1.44					
Nb/Y		0.18		0.16					
Th/Nb		0.11		0.09					

formation of the Inner Makran ocean basin or Inner Makran Spreading Zone between the Lut block and Bajgan-Dur-kan microcontinents (a southeast continuation of Sanandaj-Sirjan microcontinent) [32]. This ocean was actively spreading from early Cretaceous to early Paleocene, due to the subduction of southern Neotethys oceanic crust under the Bajgan-Dur-Kan microcontinent (in the NE or northward directions), where Kahnuj ophiolitic sequence were formed [31,32].

Our overall data show that the Dare-Anar basalts have affinities to back-arc basin environment, with Zr/Y (3.24-5.03), Th/Ta (1.29-2.55) and La/Nb ratios (1.43-2.15). The progressively enriched normalized patterns and increased Ce and Th values for the basalts (as shown in Fig. 5) also point to a back-arc basin environment for the formation of Dare-Anar basalts. This suggests that the Kahnuj ophiolitic complex displays a similar tectonic setting to other late Cretaceous Neotethyan ophiolites in the eastern Mediterranean area.

Acknowledgements

References

1. Abbate, S. G., Bortolotti, V., Paserini, P. Major structural events related to ophiolites of the Tethyan belt. *Ofioliti,* **1**: 5-32, (1979).

2. Arvin, M. Petrology and geochemistry of ophiolites and associated rocks from the Zagros suture, Neyriz, Iran. In: Maplas, J., Moores, A., Panayiotou, and Xenophonotos, C. (Eds.), Ophiolites ocean crustal analogues. *Proc. Internat. Ophiolite Symp.,* "Troodos 1987", *Geol. Surv. Dept., Cyprus Nicosia,* 351-65, (1990).

3. Arvin, M. and Robinson, P. T. The petrogenesis and tectonic setting of lava from Baft ophiolitic mélange, SW of Kerman/Iran. *Canad. J. Earth Sci.,* **31**: 824-34, (1994).

4. Arvin, M. and Shokri, E. Genesis and eruptive environment of basalts from the Gogher ophiolitic mélange, southwest of Kerman, Iran. *Ofioliti,* **22**: 175-82, (1997).

5. Bass, M. N., Moberly, R., Rhodes, J. M., Shih, C. and Church, S. E. Volcanic rocks cored in the central Pacific. Leg 17. *Init. Rep. Deep Sea Drill Proj.,* **17**: 429-503, (1973).

6. Berberian, M. and King, G. C. P. Towards a palaeogeography and tectonic evolution of Iran. *Canad. J. Earth Sci.,* **18**: 210-65, (1981).

7. Bougault, H., Joron, J. L. and Treuil, M. The primordial chondritic nature and large scale heterogeneities in the mantle: evidence from high and low partition coefficient. *Philos. Trans. R. Soc. London,* **279**: 203-13, (1980).

8. Cameron, W. E., Nisbet, E. G. and Dietrich, V. J. Petrographic dissimilarities between ophiolitic and ocean-floor basalts. In: Panayiotou, A. (Ed.), Ophiolites. *Proc. Internat. Ophiolite Symp. Geol. Surv. Dept. Cyprus Nicosia,* 182-92, (1980).

9. Coleman, R. G. *Ophiolites.* Springer, Berlin, 229 pp., (1977).

10. Dercourt, J., Zonenshian, L. P., Ricou, L. E., Kazmin, V. G., Le Pichon, X., Knipper, A. L., Grandjacquet, C., Sbortshikov, I. M., Geyssant, J., Lepvrier, C., Pechersky, D. H., Boulin, J., Sibuet, J. C., Savostin, L. A., Sorokhtin, O., Westpal, M., Bazhenov, M. L., Lauer, J. P. and Biju-Duval, B. Geological evolution of the Tethys belt from the Atlantic to the Pamirs since the Lias. *Tectonophysics,* **123**: 241-315, (1986).

11. Delaloye, M. and Desmons, J. Ophiolites and melange terranes in Iran: a geochemical study and its paleotectonic implications. *Ibid.,* **68**: 83-111, (1980).

12. Desmons, J. Meso-Cainozoic palaeogeography of the Middle East: constraints from the Iranian suture. *Geol. Alpine,* **58**: 21-30, (1982).

13. Desmons, J. and Beccaluva, L. Mid-oceanic ridge and island arc affinities in ophiolites from Iran: paleo-geographic implications. *Chem. Geol.* **39**: 39-63, (1983).

14. Floyd, P. A. Geochemical features of intraplate oceanic plateau basalts. In: Saunders, A. and Norry, M. (Eds.), Magmatism in ocean basins. *Geol. Soc. London Spec. Publ.,* **42**: 215-30, (1989).

15. Floyd, P. A., Kelling, G., Gocken, S. L., Gocken, N. Geochemistry and tectonic environment of basaltic rocks from the Miss ophiolitic melange, south Turkey. *Chem. Geol.,* **89**: 263-80, (1991).

16. Floyd, P. A. and Winchester, J. A. Identification and discrimination of altered and metamorphosed volcanic rocks using immobile elements. *Ibid.,* **21**: 291-306, (1978).

17. Frey, F. A. Bryan, W. B. Thompson, G. Atlantic ocean floor: geochemistry and petrology of basalts from Legs 2 and 3 of the Deep-Sea Drilling Project. *J. Geophys. Res.,* **79**: 5507-27, (1974).

18. Govindaraju, K. and Mevelle, G. Fully automated dissolution and separation methods for inductively coupled plasma atomic emission spectrometry rocks analysis. Application to the determination of rare earth elements. *J. Analyt. Atomic Spectrom.,* **2**: 615-21, (1987).

19. Hart, S. R., Erlank, A. J. and Kable, E. J. D. Sea floor basalts alteration: some chemical and strontium isotopic effects. *Contrib. Mineral. Petrol.* **44**: 219-30, (1974).

20. Hellman, P. L., Smith R. E. and Henderson, P. The mobility of the rare earth elements: evidence and implications from selected terrains affected by burial metamorphism. *Ibid.,* **69**: 33-47, (1979).

21. Humphris, S. E. The mobility of the rare earth elements in the crust. In: Henderson, H. (Ed.), Rare earth geochemistry. Elsvier, Amsterdam, 317-42, (1984).

22. Humphris, S. E. and Thompson, G. Trace element mobility during hydrothermal alteration of oceanic basalts. *Geochim. Cosmochim. Acta,* **42**: 127-36, (1978).

23. Hynes, A. Carbonitization and mobility of Ti, Y, and Zr in Ascot Formation metabasalts, *S. E. Quebec. Contrib. Miner. Petrol.* **75**: 79-87, (1980).

24. Keller, R. W. and Fisk, M. R. Quaternary marginal basin volcanism in Barnsfield strait as a modern analogue of the southern Chilean ophiolites. In: Parson, L. M., Murton, B. J. and Browing (Eds.), Ophiolites and their modern

oceanic analogues. *Geol. Soc. London Spec.,* **60**: 155-69, (1992).

25. Knipper, A., Ricou, L. E. and Dercourt, J. Ophiolites as indicators of the geodynamic evolution of the Tethyan ocean. *Tectonophysics,* **123**: 213-40, (1986).

26. Ludden, J. N. and Thompson, G. An evaluation of the behaviour of the rare earth elements during the weathering of the sea floor basalt. *Earth Planet. Sci. Lett.,* **43**: 85-92, (1979).

27. Marsh, N. G., Saunders, A. D., Tarney, J., and Dick, H. J. B. Geochemistry of basalts from the Shikoku and Daito basins, Deep Sea Drilling Project Leg 58. In: Klein, G. Dev. and Kobayashi, K. *et al.* (Eds.), *Init. Rep. Deep Sea Drill. Proj.* **58**: 805-42, (1980).

28. Mattews, D. H. Weathered basalts from Swallow Bank, an abyssal hill in the NE Atlantic. *Philos. Trans. R. Soc. London,* **A268**: 551-71, (1971).

29. Meschede, M. A method of discriminating between different types of mid-ocean ridge basalts and tholeiites with the Nb-Zr-Y diagram. *Chem. Geol.* **56**: 207-18, (1986).

30. Mitchell, W. S., and Aumento, F. Uranium in oceanic rocks: Deep Sea Drilling Project Leg 37. *Canad. J. Earth Sci.* **14**: 794-808, (1977).

31. McCall, G. J. H. Explanatory text of the Minab quadrangle map 1:250000, geological quadrangle No. J. 13. *Geol. Surv. Iran,* (1985).

32. McCall, G. J. H., Kidd, R. G. W. The Makran, southeastern Iran: the anatomy of a convergent plate margin active from Cretaceous to present. In: Leggett, J. (Ed), Trenchfore arc geology. *Geol. Soc. London Spec. Publ.,* **10**: 387-97, (1981).

33. Moores, E. M. Origin and emplacement of ophiolites. *Rev. Geophys. Space Phys.* **20**: 735-60, (1982).

34. Moore, J. G. Water content of basalt erupted on the sea floor. *Contrib. Mineral. Petrol.* **28**: 272-79, (1970).

35. Moore, J. G., Schilling, J. C. Vesicles, water and sulphur in Reykjanes ridge basalts. *Contrib. Mineral. Petrol.* **41**: 105-18, (1973).

36. Nicholas, A. and Jackson, E. D. Repartitions en deux provinces des peridotites des chaines alpines longeant la Mediterranee implications geotectoniques. *Bull. Swiss Min. Pet.* **52**: 479-95, (1972).

37. Pearce, J. A. Basalt geochemistry used to investigate past tectonic environments on Cyprus. *Tectonophysics,* **25**: 41-67, (1975).

38. Pearce, J. A. Geochemical evidence for the genesis and eruptive setting of lavas from Tethyan ophiolites. In: Panayiotou (Ed.), Ophiolites. *Proc. Int. Ophiolite Symp. Geol. Surv. Dept. Cyprus Nicosia,* 261-72, (1980).

39. Pearce, J. A. Trace element characteristics of lavas from destructive plate boundaries. In: Thrope, R. S. (Ed.), Andesites. John Wiley & Sons, New York, 525-48, (1982).

40. Pearce, J. A. Role of the subcontinental lithosphere in magma genesis at active continental margins. In: Hawkesworth, C. J. and Norry, M. J. (Eds.), Continental basalts and mantle xenoliths. Shiva, Nantwich, 230-49, (1983).

41. Pearce, J. A., Alabaster, T., Shelton, A. W. and Searle, M. P. The Oman ophiolite as a Cretaceous arc-basin complex: evidence and implications. *Philos. Trans. R. Soc. London,* **A300**: 299-317, (1981).

42. Pearce, J. A. and Cann, J. R. Tectonic setting of basic volcanic rocks determined using trace element analyses. *Earth Planet. Sci. Lett.,* **12**: 339-49, (1973).

43. Pearce, J. A., Lippard, S. J. and Roberts, S. Characteristics and tectonic significance of suprasubduction zone ophiolites. In: Kolelaar, B. P. and Howells, M. F. (Eds.), Marginal basin geology. *Geol. Soc. London Spec. Publ.* **16**: 77-94, (1984).

44. Pearce, J. A. and Norry, M. J. Petrogenetic implications of Ti, Zr, Y and Nb variations in volcanic rocks. *Contrib. Mineral. Petrol.* **69**: 33-47, (1979).

45. Rice-Birchall, B. and Floyd, P. A. Geochemical and source characteristics of the Tintagel Volcanic Formation. *Proc. Ussher Soc.,* **7**: 52-55, (1988).

46. Ricou, L. E. Le croissant ophiolitique peri-arabe: un ceinture de nappes mise en place au Cretace superieur. *Rev. Geogr. Phys. Geol. Dyn.,* **13**: 327-50, (1971).

47. Robertson, A. H. F. and Dixon, J. E. Introduction: aspects of the geological evolution of the eastern Mediterranean. In: Dixon, J. E. and Robertson, A. H. F. (Eds.), The geological evolution of the eastern Mediterranean. *Geol. Soc. Spec. Publ.,* **17**: 1-74, (1985).

48. Rocci, G., Ohnenstetter, D. and Ohnenstetter, M. La dualite des ophiolites tethysiennes. *Petroloogie,* **1**: 172-74, (1975).

49. Schilling, J. C. Rare earth variation across "normal segments" of the Reykjanes Ridge, 60-53°N mid-Atlantic Ridge, 29°S, the East Pacific Rise, 2-19°S, and evidence on the composition of the underlying low velocity layer. *J. Geophys. Res.* **80**: 1459-73, (1975).

50. Saunders, A. D., Tarney, J., Marsh, N. G. and Wood, D. A. Ophiolites as an ocean crust or marginal basin crust: A geochemical approach. In: Panayiotou, A. (Ed.), Ophiolites. *Proc. Internat. Ophiolite Symp. Geol. Surv. Dept. Cyprus Nicosia,* 193-204, (1980).

51. Saunders, A. D. and Tarney, J. The geochemistry of basalts from a back-arc spreading centre in the east Scotia sea. *Geochim. Cosmochim. Acta,* **43**: 555-72, (1979).

52. Saunders, A. D. and Tarney, J. Geochemical characteristics of basaltic volcanism within back-arc basins. In: Kloeaar, B. P. and Howells, M. F. (Eds.), Marginal basin geology. *Geo. Soc. London Spec. Publ.* **16**: 59-76, (1984).

53. Sengor, A. M. C. The Cimmeride orogenic system and the tectonics of Eurasia. *Geol. Soc. Am. Spec. Paper,* 195, (1984).

54. Sengor, A. M. C. Tectonics of the Tethysides: orogenenic collage development in collisional setting. *Ann. Rev. Earth Planet. Sci.* **15**: 213-44, (1987).

55. Sengor, A. M. C. A new model for the Late Palaeozoic-Mesozoic tectonic evolution of Iran and implications for Oman. *Geol. Soc. London Spec. Publ.* **49**: 797-831, (1990).

56. Shervais, J. W. Ti-V plots and the petrogenesis of modern and ophiolitic lavas. *Earth Planet. Sci. Lett.,* **59**: 101-18, (1982).

57. Smewing, J. D. and Potts, P. J. Rare earth abundances in basalts and metabasalts from the Troodos Massif, Cyprus, *Contrib. Mineral. Petrol.* **57**: 245-58, (1976).

58. Smith, R. E., Smith, S. E. Comments on the use of Ti, Zr, Y, Sr, K, P and Nb in classification of basaltic magma.

Earth Planet. Sci. Lett., **32**:114-120, (1976).

59. Sun, S. S., Nesbitt, R. W. Geochemical characteristics of mid oceanic ridge basalts. *Ibid.,* **44**: 119-38, (1979).

60. Tarney, J., Saunders, A. D., Mattey, D. P., Wood, D. A. and Marsh, N. G. Geochemical aspects of back-arc spreading in the Scotia sea and western Pacific. *Philos. Trans. R. Soc. London,* **A300**: 263-84, (1981).

61. Terrell, D. J., Pal, S., Lopez, M. M. and Perez, R. J. Rare-earth elements in basalt samples, Gulf of California. *Chem. Geol.,* **26**: 267-75, (1979).

62. Thompson, G. Metamorphic and hydrothermal processes: basalt-sea water interactions. In: Floyd, P. A. (Ed.), Ocean basalts. Blackie, Glasgow, 143-73, (1991).

63. Tirrul, R., Bell, I. R., Griffs, R. J. and Camp. V. E. The Sistan suture zone of eastern Iran. *Bull. Geol. Soc. Am.,* **94**: 134-50, (1983).

64. Venturellie, G., Thrope, R. S. and Potts, P. J. Rare earth and trace element characteristics of ophiolitic metabasalts from the Alpine-Apennine. *Earth Planet. Sci. Lett.,* **53**: 109-23, (1981).

65. Weaver, S. D., Saunders, A. D., Pankhurst, R. J. and Tarney, J. A Geological study of magmatism associated with the initial stages of back-arc spreading. The Quaternary volcanics of Bransfield Strait, from South Shetland Islands. *Contrib. Mineral. Petrol.,* **86**: 151-69, (1979).

66. White, W. M. and Bryan, W. B. Sr isotope, K, Rb, Cs, Sr, Ba and rare earth geochemistry of basalts from the FAMOUS area. *Bull. Geol. Soc. Am.,* **88**: 571-76, (1977).

67. White, W. M. and Schilling, J. G. The nature and origin of geochemical variation in Mid-Atlantic Ridge basalts from the central North Atlantic. *Geochim. Cosmochim. Acta,* **42**: 1501-16, (1978).

68. Winchester, J. A. and Floyd, P. A. Geochemical magma type discrimination: application to altered and metamorphosed basic igneous rocks. *Earth Planet. Sci. Lett.,* **28**: 459-46, (1976).

69. Winchester, J. A. and Floyd, P. A. Geochemical discrimination of different magma series and their differentiation products using immobile elements. *Chem. Geol.,* **20**: 325-43, (1977).

70. Wood, D. A., Joron, J. L. and Treuil, M. A reappraisal of the use of trace elements to classify and discriminate between magma series erupted in different tectonic settings. *Earth Planet. Sci. Lett.,* **45**: 326-36, (1979).

71. Wood, D. A., Mattey, D. P., Joron, J. L., Marsh, N. G., Tarney, J. and Treuil, M. A geochemical study of 17 selected samples from basement cores recovered at sites 447, 448, 449, 450 and 451, Deep Sea Drilling Project Leg 59. In: Orlofsky, S. (Ed.), *Init. Rep. Deep Sea Drill. Proj.,* **59**: 743-52, (1981).